

# Fault Detection of Broken Rotor Bars in Induction Motor using a Global Fault Index

G. Didier\*, E. Ternisien<sup>†</sup>, O. Caspary\*, and H. Razik<sup>†</sup>

## Abstract

Induction motors play a very important part in the safe and efficient running of any industrial plant. Early detection of abnormalities in the motor would help to avoid costly breakdowns. Accordingly, this work presents a technique for the diagnosis of broken rotor bars in induction motor. Stator voltage and current in an induction motor were measured and employed for computation of the input power of one stator phase. Waveforms of the instantaneous power and line current were subsequently analyzed using the Bartlett periodogram. We evaluate different global fault indexes on the instantaneous power spectrum and on the line current spectrum for the fault detection. Several rotor cage faults of increasing severity were studied with various load effects. Experimental results prove the efficiency of the employed method.

**keywords :** Induction Motor, Diagnosis, Bartlett Periodogram, Broken Bar, Global Modulation Index, Global Fault Index.

## 1 Introduction

Induction motors, especially the asynchronous motors, play an important part in the field of electromechanical energy conversion. It is well-known that interruptions of a manufacturing process due to a mechanical problem induces a serious financial loss for the firm. We know a variety of faults which can occur in induction machines [1] [2], such as rotor faults (broken bar or end ring) or rotor-stator eccentricity. In fact, if faults are undetected, they may lead to potentially catastrophic failures. The consequences of a faulty rotor are excessive vibrations, poor starting performances, torque fluctuation or higher thermal stress.

Various techniques have been proposed to detect a rotor fault. One of the well-known approaches for the detection of broken rotor bars in an induction machine is based on the monitoring of the stator current to detect sidebands around the supply frequency [3] - [8].

In this paper, we put forward a broken rotor bar fault detection using the power of the sidebands. The broken bar detection can be connected to the analysis of all fault components present in the line current or the instantaneous power. We estimate different global fault indexes corresponding to the contribution of all detected sidebands. We apply a non-parametric power spectrum estimation, called averaging periodograms or Bartlett method, in order to detect more precisely the frequency and the magnitude of each sideband created by the rotor fault. This method is applied on the instantaneous power of one stator phase and on its line current when the motor is connected directly to the supply voltage.

Scientists have already used the instantaneous power spectral analysis for the diagnosis of broken rotor bar. For example, in 1999, Cruz calculated the ratio of the magnitude of the characteristic component  $2sf_s$  and the DC (Direct Current) level of the power. He showed that this severity factor is independent of motor rating and motor-load inertia [9]. In 1996 and 2000, Legowski *et al.* [10] Trzynadlowski and Ritchie [11] compared the partial and total instantaneous power to the line current and concluded that the latter yields inferior results to the first for broken rotor bars detection and mechanical abnormalities in induction motor.

The advantages of the use of the instantaneous power spectrum are given as follows:

- presence of additional components in low frequencies;
- first low frequency component is positioned directly at the speed oscillation frequency;

---

\*Groupe de Recherche en Electrotechnique et Electronique de Nancy, GREEN-CNRS UMR-7037, Université Henri Poincaré, 54506 Vandœuvre-lès-Nancy Cedex, France. e-mail: gaetan.didier@green.uhp-nancy.fr; hubert.razik@green.uhp-nancy.fr

<sup>†</sup>Centre de Recherche en Automatique de Nancy, CRAN-CNRS UMR-7039, Université Henri Poincaré, 54506 Vandœuvre-lès-Nancy Cedex, France. e-mail: eric.ternisien@iutds.uhp-nancy.fr; olivier.caspary@iutds.uhp-nancy.fr

- easier filtering of the DC component in the power spectrum than to remove the 50 Hz fundamental component in the current spectrum without affecting the components at  $(1 \pm 2s)f_s$  in case of a very little slip ( $s$  represents the slip of the machine and  $f_s$  the supply frequency).

The method exposed in this paper, in comparison to the works quoted previously, uses all components created by the rotor fault in the instantaneous power spectrum for the final diagnosis. We show that additional information carried by the instantaneous power in low frequency improves the diagnosis of broken rotor bars. In fact, such an instantaneous power method can be interpreted as a modulation operation in the time domain that translates the spectral components specific to the broken rotor bar to a [0-50] Hz frequency well-bounded [12] [13]. We show that the diagnosis of a partially broken rotor bar ( $\simeq$  half broken bar) can be carried out even if the motor operates under low load.

## 2 The instantaneous power signature

First of all, we consider an ideal three phase supply voltage. The instantaneous power  $p_s(t)$  of one phase is classically given by:

$$p_s(t) = v_s(t)i_s(t) \quad (1)$$

where  $v_s(t)$  is the instantaneous line voltage and  $i_s(t)$  stands as its line current. If those two conditions are respected, the supply voltage is sinusoidal and the speed is constant (no ripple). The instantaneous power can be written as follows:

$$v_s(t) = \sqrt{2}V_s \cos(\omega t) \quad (2)$$

$$i_{s0}(t) = \sqrt{2}I_s \cos(\omega t - \varphi) \quad (3)$$

$$p_{s0}(t) = V_s I_s [\cos(2\omega t - \varphi) + \cos \varphi] \quad (4)$$

where  $\varphi$  is the phase angle between the voltage and the current line. The power spectrum of the current has only one fundamental component at the frequency  $f_s = \omega/(2\pi)$ , while the instantaneous power spectrum has a DC component and its fundamental component at the frequency  $2f_s = (2\omega)/(2\pi)$ .

When a bar breaks, a rotor asymmetry occurs. The result is the appearance of a backward rotating field at the slip frequency  $gf_s$  with respect to the forward rotating rotor. It induces in the stator current an additional frequency at  $f_{bb_s} = (1 - 2s)f_s$ . This cyclic current variation implies a speed oscillation and a torque pulsation at the twice slip frequency ( $2sf_s$ ). This speed oscillation induces, in the stator winding, an upper component at  $f_{bb_{h,s}} = (1 + 2s)f_s$ . Briefly, broken rotor bars induce in the stator winding additional components at frequencies given by:

$$f_{bb_s} = (1 \pm 2ks)f_s \quad (5)$$

where  $k = 1, 2, 3, \dots$

Therefore, the current is modulated and can be written as follows [13]:

$$i_s(t) = i_{s0}(t) \left[ 1 + \sum_h M_{ch} \cos(h\omega_f t) \right] \quad (6)$$

$$\begin{aligned} i_s(t) = & i_{s0}(t) + \sum_h \frac{\sqrt{2}M_{ch}I_s}{2} [\cos((\omega - h\omega_f)t - \varphi) \\ & + \cos((\omega + h\omega_f)t - \varphi)] \end{aligned} \quad (7)$$

where  $M_{ch}$  denotes the modulation depth (modulation index) and  $h = 1, 2, 3, \dots$

The last expression considers that the magnitude of the left and the right components are identical for the same index  $h$ . If we take a look at Fig. 1(a) and 1(b) which represents the line current spectrum with a healthy rotor and one broken bar, we can see that components at  $f_{bb_s} = (1 - 2ks)f_s$  do not have the same magnitude as components at  $f_{bb_s} = (1 + 2ks)f_s$  for the same index  $h$  (influence of the load inertia). Consequently, we have to separate the magnitude of the left and the right components in expression (7) by introducing a index for each

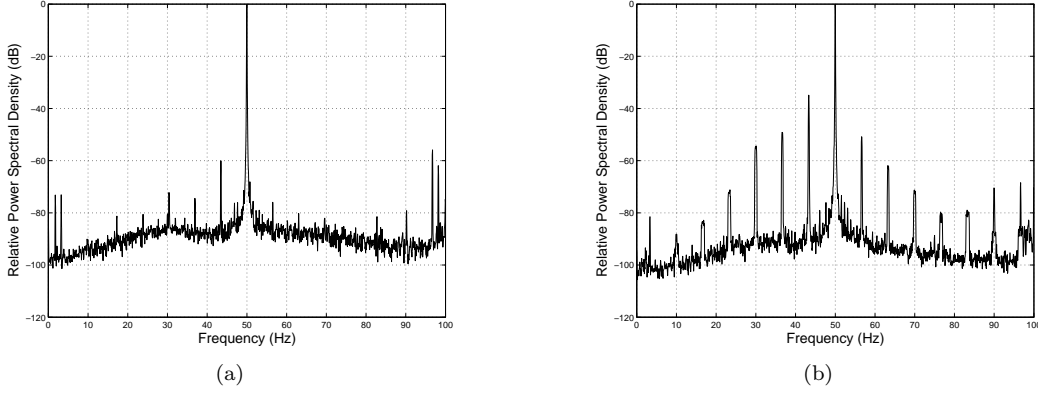


Figure 1: Current spectrum for a healthy rotor (a) and one broken rotor bar (b).

component (this index is called magnitude index to make a distinction with the modulation index presents in (6)). The new expression of the modulated current is given by:

$$\begin{aligned}
 i_s(t) &= i_{s0}(t) + \sum_k \frac{\sqrt{2}M_{c_k}I_s}{2} \cos((\omega - k\omega_f)t - \varphi) \\
 &\quad + \sum_k \frac{\sqrt{2}M'_{c_k}I_s}{2} \cos((\omega + k\omega_f)t - \varphi)
 \end{aligned} \tag{8}$$

where  $M_{c_k}$  denotes the magnitude index for left components,  $M'_{c_k}$  denotes the magnitude index for right components and  $f_f = \frac{\omega_f}{2\pi} = 2sf_s$  acts as the modulation frequency. If we develop the cosinus terms, we can put this last expression in the form:

$$\begin{aligned}
 i_s(t) &= i_{s0}(t) + \sum_k \frac{\sqrt{2}I_s}{2} (M_{c_k} + M'_{c_k}) \cos(k\omega_f t) \\
 &\quad (\cos \varphi \cos(\omega t) + \sin \varphi \sin(\omega t)) \\
 &\quad + \sum_k \frac{\sqrt{2}I_s}{2} (M_{c_k} - M'_{c_k}) \sin(k\omega_f t) \\
 &\quad (\cos \varphi \sin(\omega t) - \sin \varphi \cos(\omega t))
 \end{aligned} \tag{9}$$

This expression allows us to find a similarity with (6) given previously. We can see in (9) that, if we consider only the study of the magnitude, we define two new indexes:

$$M_{cm_k} = \frac{(M_{c_k} + M'_{c_k})}{2} \tag{10}$$

$$M_{co_k} = \frac{(M_{c_k} - M'_{c_k})}{2} \tag{11}$$

The first corresponds to the modulation index usually used in the signal theory, and the second will be called in this paper oscillation index. Fig. 2(a) and Fig. 2(b) show us a theoretical spectrum to explain the origin of the different indexes used in (8) and (9).

The mathematical expression for the modulated instantaneous power of one phase is obtained by multiplying (2) by (8) and is written:

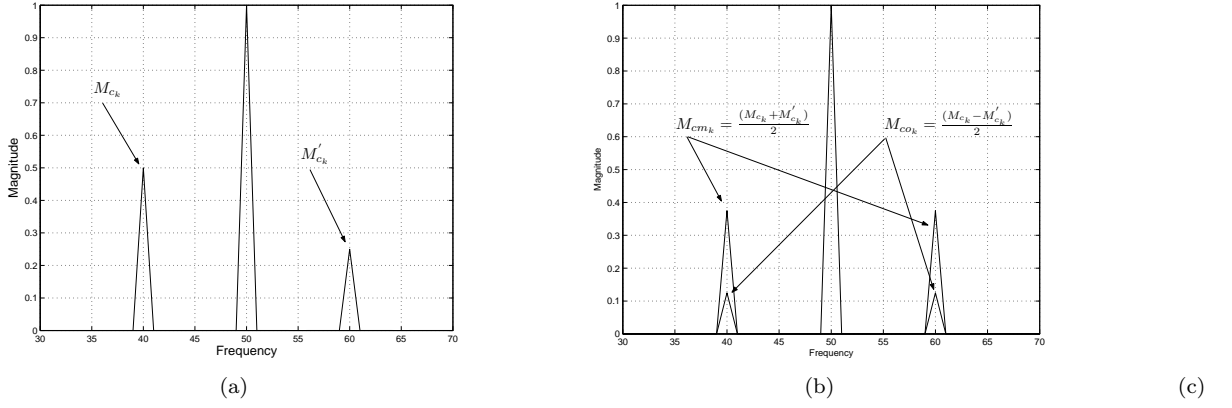


Figure 2: Magnitude indexes of the left and right component (a), modulation index  $M_{cm_k}$  and oscillation index  $M_{co_k}$  (b)

$$\begin{aligned}
p_s(t) &= p_{s0}(t) + \sum_k \frac{M_{p_k} V_s I_s}{2} \cos((2\omega - k\omega_f)t - \varphi) \\
&+ \sum_k \frac{M'_{p_k} V_s I_s}{2} \cos((2\omega + k\omega_f)t - \varphi) \\
&+ \sum_k \frac{V_s I_s}{2} [M_{p_k} + M'_{p_k}] \cos \varphi \cos(k\omega_f t) \\
&+ \sum_k \frac{V_s I_s}{2} [M'_{p_k} - M_{p_k}] \sin \varphi \sin(k\omega_f t)
\end{aligned} \tag{12}$$

In addition to the fundamental frequency and sideband components at  $f = (2\omega \pm \omega_f)/(2\pi)$  for the case of  $k = 1$ , we have a spectral peak at the modulation frequency  $f_f = \omega_f/(2\pi)$  in the instantaneous power spectrum. The latter, referred to the characteristic component, provides an additional indication of diagnosis information about the state of the motor. Its amplitude depends on phase angle  $\varphi$  and on indexes  $M_{p_1}$  and  $M'_{p_1}$ . In our case, this component is used for the calculation of the  $2sf_s$  frequency. This value could be used for the induction machine speed estimation. If we rewrite (12) in the same form as (9), we obtain for the expression of the modulation index  $M_{pm_k}$  and for the oscillation index  $M_{po_k}$  of the instantaneous power, the following expressions:

$$M_{pm_k} = \frac{(M_{p_k} + M'_{p_k})}{2} \tag{13}$$

$$M_{po_k} = \frac{(M_{p_k} - M'_{p_k})}{2} \tag{14}$$

The value of magnitude indexes  $M_{c_k}$ ,  $M'_{c_k}$ ,  $M_{p_k}$  and  $M'_{p_k}$  depends on the severity of the abnormality. In fact, these indexes will increase when a broken bar appears because magnitudes of the different components created by the rotor fault will increase. We could use this information for the broken rotor bars diagnosis of induction motor.

### 3 Broken bar detection based on the global fault index

In the case of a healthy motor, the equation of the instantaneous power contains an amplitude modulation with one modulation signal around the carrier frequency at 100 Hz. In fact, this modulation signal is created by a natural rotor asymmetry (eccentricity created by the load for example). If a broken rotor bar occurs, this asymmetry increases and several sidebands appear at the modulation frequency  $2ksf_s$ . According to the amplitude modulation theory, if several sinusoidal signals modulate the same carrier wave, the power of this wave does not change while the modulating signals increase the power contained in sidebands. Since the modulation

index is proportional to the amplitude of the modulating signal, different modulation indexes correspond to different modulating signals. The global modulation index  $M_{gm_x}$  is defined as that the power of sidebands equals the sum of powers of each sideband:

$$\frac{M_{gm_x}^2 P_c}{2} = \sum_k \frac{M_{xm_k}^2 P_c}{2} \quad (15)$$

where the spectral power  $P_c$  of the carrier frequency is  $P_c = (V_s I_s)^2$  with the signal  $p_s(t)$ . The subscript letter  $x$ , in the latter expression, can be replaced by  $p$  (instantaneous power) or  $c$  (line current). For the global oscillation index  $M_{go_x}$ , we have:

$$\frac{M_{go_x}^2 P_c}{2} = \sum_k \frac{M_{xo_k}^2 P_c}{2} \quad (16)$$

If we have a look at (8) and (12), we propose to calculate a new index that we call global fault index  $M_{tx}$  with the expression:

$$\frac{M_{tx}^2 P_c}{2} = \sum_k \frac{M_{xk}^2 P_c}{2} + \sum_k \frac{M'_{xk}{}^2 P_c}{2} \quad (17)$$

This expression was chosen so as to find a similarity with the signal theory. The expression of  $M_{tx}$ , by supposing  $K_l$  the number of components at the left of the supply frequency and  $K_r$  the number of components at the right, becomes:

$$M_{tx}^2 = \sum_{k=1}^{K_l} M_{xk}^2 + \sum_{k=1}^{K_r} M'_{xk}{}^2 \quad (18)$$

Moreover, for each modulation frequency ( $2f_s \pm 2ksf_s$ ) for the instantaneous power spectrum and ( $f_s \pm 2ksf_s$ ) for the line current spectrum, we can deduce its magnitude index  $M_z$  by dividing its estimated amplitude  $A_{s_z} = M_z A_c / 2$  by the amplitude of the carrier frequency  $A_c = V_s I_s$  ( $z$  can be replaced by  $c_k$  for the line current and  $p_k$  for the instantaneous power):

$$\begin{aligned} \frac{A_{s_z}}{A_c} &= \frac{M_z A_c}{2} \frac{1}{A_c} = \frac{M_z}{2} \\ M_z &= \frac{2A_{s_z}}{A_c} \end{aligned} \quad (19)$$

The same method can be applied for the low frequency components of the instantaneous power. In fact, we have seen previously that instantaneous power spectrum contains additional components in low frequency. We can use the magnitude of these components to determine their global fault index. With (12), we can give the mathematical relation of the low frequency components magnitude for a specific value of  $k$ :

$$A_{p_k} = \sum_k \frac{V_s I_s}{2} \sqrt{M_{p_k}^2 + M'_{p_k}{}^2 + 2M_{p_k} M'_{p_k} \cos(2\varphi)} \quad (20)$$

where  $A_{p_k}$  denotes the magnitude of the low frequency component  $k$  presents in the instantaneous power spectrum. With the latter expression, we can deduce a new fault index  $M_{lf_k}$  specific to those components:

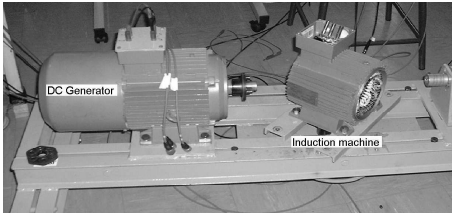
$$M_{lf_k} = \sqrt{M_{p_k}^2 + M'_{p_k}{}^2 + 2M_{p_k} M'_{p_k} \cos(2\varphi)} \quad (21)$$

and consequently, we can deduce the global fault index for the low frequency components with the expression:

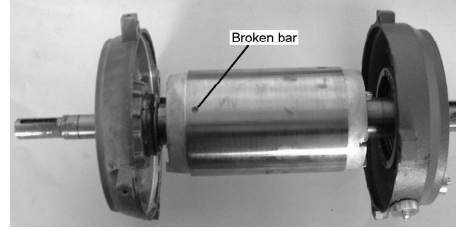
$$M_{t_{lf}}^2 = \sum_{k=1}^{K_{pn}} M_{lf_k}^2 \quad (22)$$

where  $K_{pn}$  represents the number of components detected in the low frequency band.

Thus, the broken bar detection can be connected to the analysis of the global modulation index  $M_{gm_x}$ , the global oscillation index  $M_{go_x}$ , the global fault index  $M_{tx}$  and the low frequency global fault index  $M_{t_{lf}}$ . If a fault appears in the rotor cage, we will have an increase of those global indexes and consequently, a good indication for the diagnosis of the motor. To evaluate those global indexes, we must find the frequency and amplitude of each sideband to estimate the magnitude indexes  $M_{xk}$ ,  $M'_{xk}$  and  $M_{lf_k}$ .

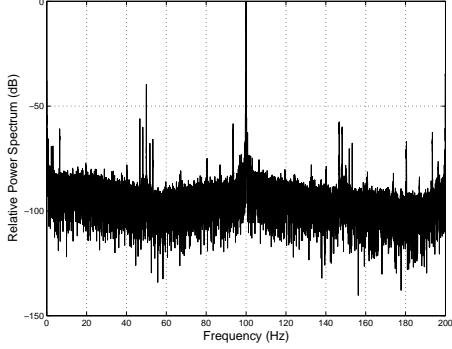


(a)

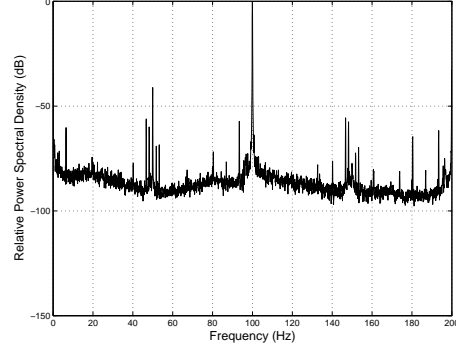


(b)

Figure 3: Test-bed (a) and position of the broken rotor bar (b).



(a)



(b)

Figure 4: Classic periodogram (a) and Bartlett periodogram (b) of  $p_s(t)$  for the healthy rotor.

To reduce the variance in the spectrum and to improve the evaluation of the components magnitude, we apply a non-parametric power spectrum estimation, called averaging periodograms or Bartlett method, instead of the classic periodogram [15]. Indeed, when the record length  $N$  increases, the frequency resolution of the periodogram is better but its variance is not reduced. The definition of the periodogram is:

$$\hat{P}_{p_s}(f) = \frac{1}{N} \left| \sum_{m=0}^{N-1} \omega(m) p_s(m) e^{-j2\pi f m} \right|^2 \quad (23)$$

and it can be calculated from a Discrete Fourier Transform (DFT) or a Fast Fourier Transform (FFT). We can use a window  $\omega(m)$  if necessary to form the modified periodogram. For the Bartlett periodogram, the data sequence of  $N$  samples is divided into  $L$  non-overlapping segments of  $D$  samples such as  $D \cdot L < N$ . The modified periodograms of each segment are averaged in order to reduce the variance of the Bartlett periodogram as follows [16]:

$$\hat{P}_{p_s}^B(f) = \frac{1}{L} \sum_{i=0}^{L-1} \hat{P}_{p_s}^{(i)}(f) \quad (24)$$

where  $\hat{P}_{p_s}^{(i)}(f)$  is the modified periodogram of the  $i^{\text{th}}$  segment of the signal  $p_s(m)$ . Overlapped segments can be used to form the Welch periodogram but it is not necessary in our case because of the high number of samples.

Nevertheless, the Bartlett periodogram is only fitted for the use with an operation at steady state as it is the case in this study.

## 4 Experimental results

The test-bed used in the experimental investigation is composed of a three-phase induction motor, 50 Hz, 2 poles, 3kW (Fig. 3(a)). In order to test the effectiveness of the suggested method, we have several identical rotors with 28 bars which can be exchanged without affecting the electrical and magnetic features. The position of the broken bar is given on Fig. 3(b). The voltage and the line current measurements were made at the nominal rate. For those two variables, the sampling frequency was 2 kHz and each data length was equal to  $2^{18}$  values.

Table 1: CALCULATION OF DIFFERENT GLOBAL INDEXES

Motor	$2sf_s$ frequency	Speed (r/min)	$K_{pn}$	$M_{t_{lf}}$	$M_{t_p}$	$M_{t_c}$	$M_{gm_p}$	$M_{go_p}$	$M_{gm_c}$	$M_{go_c}$
H-L100	6.53	2804	2	0.0020	0.0028	0.0021	0.0015	0.0012	0.0012	0.0009
05b-L100	5.98	2820	3	0.0063	0.0060	0.0058	0.0037	0.0021	0.0033	0.0018
1b-L100	6.67	2799	3	0.0435	0.0454	0.0408	0.0260	0.0189	0.0237	0.0164
H-L75	4.94	2851	3	0.0024	0.0036	0.0024	0.0021	0.0015	0.0014	0.0008
05b-L75	4.27	2871	3	0.0057	0.0064	0.0051	0.0040	0.0021	0.0032	0.0015
1b-L75	4.64	2860	4	0.0408	0.0470	0.0442	0.0288	0.0165	0.0274	0.0151
H-L50	3.17	2904	2	0.0017	0.0023	0.0018	0.0015	0.0007	0.0012	0.0004
05b-L50	2.87	2913	3	0.0040	0.0057	0.0038	0.0037	0.0017	0.0026	0.0007
1b-L50	2.99	2910	4	0.0279	0.0393	0.0350	0.0256	0.0109	0.0233	0.0083
H-L25	1.59	2952	2	0.0044	0.0100	0.0048	0.0059	0.0038	0.0030	0.0014
05b-L25	1.47	2956	2	0.0115	0.0214	0.0100	0.0120	0.0092	0.0061	0.0036
1b-L25	1.53	2954	3	0.0240	0.0358	0.0281	0.0246	0.0059	0.0198	0.0019

We can see in Fig. 4(a) and Fig. 4(b), which represent the power spectrum of the instantaneous power of one phase for the healthy rotor (referred to the 100 Hz fundamental), that the noise level is reduced thanks to the averaging by using the Bartlett periodogram (the data length  $D$  for the average is equal to  $2^{15}$  values). We have shown in [17] that the use of a Hanning's window for the calculation of the Bartlett periodogram ( $\omega(m)$  in (23)) improves the detection of the components magnitude for the evaluation of magnitude indexes  $M_{c_k}$ ,  $M'_{c_k}$ ,  $M_{p_k}$  and  $M'_{p_k}$ .

We keep a good estimation of the sidebands power translated from the 0 Hz by avoiding numerous maxima peaks contained in each one because of a very slight frequency variation of the slip. Consequently, we can consider the detection of maxima peaks in the spectrum. The first frequency that we want to detect is the  $2sf_s$  frequency because it corresponds to the component with the highest power that is not disrupted by the supply power when we remove the mean of the instantaneous power signal. Then, we search all maxima from this first frequency that are at frequencies  $2ksf_s$  in the considered band [1 – 35] Hz with a greater accuracy (the tolerance is below 1%) and above a threshold defined as the mean of this spectral band. This information gives us the number of components  $K_{pn}$  and the magnitude of each one. With those magnitudes, we can calculate the global modulation index  $M_{lf_k}$  specific to the low frequency components with (22). The value  $K_{pn}$ , multiplied by two, gives us the total number of components that we must detect on both sides of the carrier frequency of  $p_s(t)$  and  $i_s(t)$ . We calculate the frequencies  $2(1 \pm ks)f_s$  in the instantaneous power spectrum and  $(1 \pm 2ks)f_s$  in the current spectrum to evaluate their magnitudes. Then, we estimate the magnitude index of each modulation frequency in the same way as (19). At the end, with (15), (16), (18) and (22), we can calculate the global modulation index  $M_{gm_c}$ , the oscillation index  $M_{go_c}$  and the global fault index  $M_{t_c}$  specific to the line current spectrum and the global modulation index  $M_{gm_p}$ , the oscillation index  $M_{go_p}$ , the global fault index  $M_{t_p}$  and the low frequency global fault index  $M_{t_{lf}}$  specific to the instantaneous power spectrum. We made a comparison between those seven various indexes in the continuation of paper to find which is the most judicious to base the diagnosis of broken rotor bars.

We studied the case of a partially broken rotor bar and one broken rotor bar with different load levels. Table 1 shows the results obtained by the proposed method. In this Table, we report the state of the motor (for example we note H-L100 the case of a healthy rotor with 100% load and 05b-L25 the case of a partially broken rotor bar with 25% load), the value of the  $2sf_s$  frequency, the speed of the motor, the peaks number  $K_{pn}$  found in the band [1 - 35] Hz, the value of the three different global fault indexes, the value of the two different global modulation indexes and finally the value of the two different global oscillation indexes.

Fig. 5(a) and 5(b) represent the line current and the instantaneous power spectra for a healthy rotor. We can note that instantaneous power spectrum contains a modulation frequency at  $2sf_s$  (which is induced by a natural eccentricity of the rotor) and a component at the frequency  $2(1 - s)f_s$ . This component is also present in the line current spectrum at the frequency  $(1 - 2s)f_s$ . The same phenomenon appears in Fig. 7(a) and 7(b) for 25% load. This modulation frequency allows the calculus of global indexes in the case of a healthy rotor. Those indexes will stand as a reference for the broken rotor bar diagnosis.

Table 2: COMPARISON BETWEEN DIFFERENT GLOBAL FAULT INDEXES.

Motor	$K_{pn}$	$M_{t_{lf}}$	$\alpha M_{t_{lf}}$	Color	$M_{t_p}$	$\alpha M_{t_p}$	Color	$M_{t_c}$	$\alpha M_{t_c}$	Color
H-L100	2	0.0020	0.0040	G	0.0028	0.0056	G	0.0021	0.0042	G
05b-L100	3	0.0063	0.0040	R	0.0060	0.0056	R	0.0058	0.0042	R
1b-L100	3	0.0435	0.0040	R	0.0454	0.0056	R	0.0408	0.0042	R
H-L75	3	0.0024	0.0048	G	0.0036	0.0072	G	0.0024	0.0048	G
05b-L75	3	0.0057	0.0048	O	0.0064	0.0072	<b>G</b>	0.0051	0.0048	O
1b-L75	4	0.0408	0.0048	R	0.0470	0.0072	R	0.0442	0.0048	R
H-L50	2	0.0017	0.0034	G	0.0023	0.0046	G	0.0018	0.0036	G
05b-L50	3	0.0040	0.0034	R	0.0057	0.0046	R	0.0038	0.0036	R
1b-L50	4	0.0279	0.0034	R	0.0393	0.0046	R	0.0350	0.0036	R
H-L25	2	0.0044	0.0088	G	0.0100	0.0200	G	0.0048	0.0096	G
05b-L25	2	0.0115	0.0088	O	0.0214	0.0200	O	0.0100	0.0096	O
1b-L25	3	0.0240	0.0088	R	0.0358	0.0200	R	0.0281	0.0096	R

Table 3: COMPARISON BETWEEN DIFFERENT GLOBAL MODULATION INDEXES AND GLOBAL OSCILLATION INDEXES.

Motor	$K_{pn}$	$M_{gm_p}$	$\alpha M_{gm_p}$	C	$M_{go_p}$	$\alpha M_{go_p}$	C	$M_{gm_c}$	$\alpha M_{gm_c}$	C	$M_{go_c}$	$\alpha M_{go_c}$	C
H-L100	2	0.0015	0.0030	G	0.0012	0.0024	G	0.0012	0.0024	G	0.0009	0.0018	G
05b-L100	3	0.0037	0.0030	R	0.0021	0.0024	<b>G</b>	0.0033	0.0024	R	0.0018	0.0018	R
1b-L100	3	0.0260	0.0030	R	0.0189	0.0024	R	0.0237	0.0024	R	0.0164	0.0018	R
H-L75	3	0.0021	0.0042	G	0.0015	0.0030	G	0.0014	0.0028	G	0.0008	0.0016	G
05b-L75	3	0.0040	0.0042	<b>G</b>	0.0021	0.0030	<b>G</b>	0.0032	0.0028	O	0.0015	0.0016	<b>G</b>
1b-L75	4	0.0288	0.0042	R	0.0165	0.0030	R	0.0274	0.0028	R	0.0151	0.0016	R
H-L50	2	0.0015	0.0030	G	0.0007	0.0014	G	0.0012	0.0024	G	0.0004	0.0008	G
05b-L50	3	0.0037	0.0030	R	0.0017	0.0014	R	0.0026	0.0024	R	0.0007	0.0008	<b>G</b>
1b-L50	4	0.0256	0.0030	R	0.0109	0.0014	R	0.0233	0.0024	R	0.0083	0.0008	R
H-L25	2	0.0059	0.0118	G	0.0038	0.0076	G	0.0030	0.0060	G	0.0014	0.0028	G
05b-L25	2	0.0120	0.0118	O	0.0092	0.0076	O	0.0061	0.0060	O	0.0036	0.0028	O
1b-L25	3	0.0246	0.0118	R	0.0059	0.0076	<b>G</b>	0.0198	0.0060	R	0.0019	0.0028	<b>G</b>

Table 4: INCREASE OF GLOBAL FAULT INDEXES  $M_{t_{lf}}$ ,  $M_{t_c}$  AND  $M_{gm_c}$ .

Motor	$M_{t_{lf}}$	$M_{t_c}$	$M_{gm_c}$
05b-L100	215 %	176 %	175 %
1b-L100	2075 %	1842 %	1875 %
05b-L75	137 %	112 %	128 %
1b-L75	1600 %	1741 %	1857 %
05b-L50	135 %	111 %	116 %
1b-L50	1541 %	1844 %	1841 %
05b-L25	161 %	108 %	103 %
1b-L25	445 %	485 %	560 %



We can see in Fig. 6(a) and 6(b) for 100% load and Fig. 8(a) and 8(b) for 25% load that when a rotor fault appears, the components created by the asymmetry increase in magnitude in the line current and instantaneous power spectra. We see in Table 1 that, in the case of one broken rotor bar, global fault indexes, global modulation indexes and global oscillation indexes increase in a very significant way. For a partially broken rotor bar, these indexes increase but with a less significant value than for the test with one broken rotor bar. Moreover, Table 1 shows us that the number of peaks  $K_{pn}$  detected in the low frequency band of the instantaneous power spectrum also increases with the rotor fault.

Consequently, for the broken rotor bar diagnosis, we established a criterion which takes into account global indexes (modulation, oscillation and fault) and peaks number  $K_{pn}$ . This criterion is given at Table 5. Index

Table 5: CRITERION USED FOR THE FAULT DETECTION.

Test	Result
$if (M_{X_{Measured}} < \alpha M_{X_{Healthy}})$	No fault (Green color)
$if (M_{X_{Measured}} \geq \alpha M_{X_{Healthy}}) \& (K_{pn_{Measured}} = K_{pn_{Healthy}})$	Incipient rotor fault (Orange color)
$if (M_{X_{Measured}} \geq \alpha M_{X_{Healthy}}) \& (K_{pn_{Measured}} > K_{pn_{Healthy}})$	Rotor Fault (Red color)

$M_X$  represents one of the seven global indexes ( $M_{gm_p}$ ,  $M_{go_p}$ ,  $M_{gm_c}$ ,  $M_{go_c}$ ,  $M_{t_{lf}}$ ,  $M_{t_p}$  or  $M_{t_c}$ ). The term  $\alpha$  is called index of sensitivity and takes value 2 in this case ( $\alpha = 2$ ).

Table 2 gives us the results of the criterion explained previously applied to the three global fault indexes. The last column is composed of colors as Green, Orange and Red as preciously mentioned. With the use of the global fault index  $M_{t_p}$ , the criterion does not detect the incipient rotor fault (partially broken rotor bar) with 75% load. With global fault indexes  $M_{t_{lf}}$  and  $M_{t_c}$ , the detection of rotor faults is possible in all cases. If we have a look at Table 3 which gives the results of the criterion applied to global modulation indexes and to global oscillation indexes, we can deduce that only the global modulation  $M_{gm_c}$  allows the detection of all faults. Global index  $M_{gm_p}$  does not detect a partially broken rotor bar with 75% load. In the case of global index  $M_{go_p}$ , it is a partially broken rotor bar with 75% and 100% load and one broken rotor bar with 25% load which are not detected. Moreover, if we refer to global oscillation index  $M_{go_c}$ , it is a partially broken rotor bar with 50% and 75% load and one broken rotor bar with 25% load which are not detected.

According to the latter notes, only the low frequency global fault index of the instantaneous power  $M_{t_{lf}}$ , the global fault index  $M_{t_c}$  and the global modulation index  $M_{gm_c}$  of the line current allow the detection of all faults. Table 4 shows the increase of those three global fault indexes for each defect. We can deduce that the global fault index specific to the low frequency of the instantaneous power spectrum  $M_{t_{lf}}$  allows a detection of the partially broken rotor bar faster than global fault indexes of the line current  $M_{t_c}$  and  $M_{gm_c}$  because it increases more significantly.

Consequently, we advocate the use of the global fault index  $M_{t_{lf}}$  specific to the low frequency components of the instantaneous power of one stator phase for the broken rotor bar diagnosis in induction motor. Besides, with the exposed method, an incipient rotor fault generated by a partially broken rotor bar in the rotor cage with 25% load has been detected. With a load inferior to 25%, the broken rotor bar detection remains difficult with this method because the instantaneous power of the motor is absorbed by the stator (stator ohmic losses and stator core losses). The power transmitted to the rotor is very low. However, if we consider the fact that in industrial applications, the motors operate with a load level higher than 50%, the presented method exposed gives very good information about the state of the rotor cage.

If we make a comparison to other techniques such as pattern recognition [18] or neural networks ones, this approach presents some advantages. First, our method does not need a training to create a classifier (only a few tests with a healthy rotor at a specific load are needed). Consequently, it is not necessary to make a lot of tests to obtain training samples. Moreover, the method allows the detection of an incipient rotor fault (0.5/28 bars). This point may be difficult since the two classes (healthy and half broken bar) are very close to each other, and decision is difficult to take. Finally, if we consider the case of a DSP implementation, the computational time is faster (only a FFT calculus and a few operations).

## 5 Conclusion

In this paper, a novel approach of diagnosis on induction motor has been put forward and tested. The diagnosis based on the global fault index method applied to the instantaneous power signal and line current signal provides

relevant results for the detection of broken rotor bars. A comparison between those two signals allowed to show that the detection of a partially broken rotor bar is faster if we use the low frequency global fault index of the instantaneous power. We have demonstrated that a half broken bar with 25% load can be detected using the criterion which has been developed previously. The experimental results showed up the effectiveness of the technique, even if the motor operates under a low load.

We can note that this method can be used for the detection of mechanical faults (for example, pulsation torque at the twice slip frequency). In this case, the components present around the supply frequency of the line current and instantaneous power have the same frequencies than the components created by a broken rotor bar fault. In addition to components present around the supply frequency, it is well known that rotor cage fault creates additional components at frequencies  $(\frac{k}{p}(1-s) \pm s)f_s$ , where  $\frac{k}{p}$  denotes the space harmonic number (3, 5, 7, ...) [19]. The evaluation of a new global fault index, specific to the components present near to space harmonics could be done. In fact, we know that when a mechanical fault appears, contrary to a rotor fault, those components are not disrupted. Indeed, a broken rotor bar induces a modification of the rotor induction (fundamental and space harmonics) what results in an increase of components harmonics amplitude in the line current spectrum. This phenomenon does not appear in the case for a load torque variation. With this study, we could differentiate a mechanical fault from a rotor fault with a good accuracy [20].

The method can also be extended to the detection of eccentricity faults. A new fault index, specific to static and/or dynamic eccentricities can be created by monitoring components situated at frequencies [21]:

$$f_{sh} = \left[ (kR \pm n_d) \frac{(1-s)}{p} \pm v \right] f_s \quad (25)$$

where  $k = 0, 1, 2, \dots$ ;  $R$  is the number of rotor slots;  $n_d$  is know as eccentricity order and  $v = \pm 1, \pm 3, \dots$  is the order of stator time harmonics that are present in the power supply. If the index increases with regards to the healthy rotor reference, an eccentricity fault is detected.

Finally, in order to make  $\alpha$  independent of machine parameters, additional tests with different motors will be necessary.

## 6 Parameters of motor used in experiments

Number of poles	2
Rated power	3 kW
Rated voltage	230 Volts
Rated current	5.90 Amp
Rated frequency	50 Hz
Rated speed	2800 r/min
Number of stator slots	36
Number of rotor bars	28

## Acknowledgment

The authors wish to express their gratefulness to the Ministère de la Recherche and to the Université Henri Poincaré of Nancy for their financial support in the development of the test-bed.

## References

- [1] A.H. Bonnet, "Analysis of Rotor Failures in Squirrel Cage Induction Machines," *IEEE Trans. on Industry Applications*, vol. 24, No 6, pp. 1124–1130, Nov./Dec. 1988.
- [2] A.H. Bonnet and G.C. Soukup, "Cause and Analysis of Stator and Rotor Failures in Three-Phase Squirrel-Cage Induction Motors," *IEEE Trans. on Industry Applications*, vol. 28, No 4, pp. 921–937, July/August 1992.
- [3] S. Nandi and H.A. Toliyat, "Fault Diagnosis of Electrical Machine - A Review," in *IEMDC'99*, pp. 219–221, May 1999.

- [4] W.T. Thomson and M. Fenger, "Current Signature Analysis to Detect Induction Motor Faults," *IEEE Trans. on IAS Magazine*, Vol. 7, No. 4, pp. 26–34, July/August 2001.
- [5] G.B. Kliman and J. Stein, "Induction motor fault detection via passive current monitoring," in *Proc. ICEM'90*, Vol. 1, pp. 13–17.
- [6] G.B. Kliman, J. Stein, R. D. Endicott and R. A. Koegl, "Noninvasive Detection of Broken Rotor Bars in Operating Induction Motor," in *IEEE Trans. on Energy Conversion*, Vol. 3, No. 4, pp. 873–879, Dec. 1998.
- [7] G. Didier and H. Razik and A. Rezzoug, "On the Modelling of Induction Motor Including the First Space Harmonics for Diagnosis Purposes," *International Conference on Electrical Machine ICEM'02*, August 2002.
- [8] G. Didier and H. Razik and A. Abed and A. Rezzoug, "On Space Harmonics Model of a Three Phase Squirrel Cage Induction Motor for Diagnosis Purposes," *International Power Electronics and Motion Control Conference EPE-PEMC'02*, Croatia, Sept. 2002.
- [9] S. M. A. Cruz, A. J. Marques Cardoso, "Rotor Cage Fault Diagnosis in Three Phase Induction Motors by the Total Instantaneous Power Spectral Analysis," in *IAS Annual Meeting Conference*, Vol. 3, pp. 1929–1934, Oct. 3-7, 1999.
- [10] S.F. Legowski and A.H.M. Sadrul Ula and A.M. Trzynadlowski, "Instantaneous Power as a medium for the Signature Analysis of Induction Motors," *IEEE Trans. on Industry Electronics*, Vol. 47, No 5, pp. 984–993, Oct. 1996.
- [11] A.M. Trzynadlowski and E. Ritchie, "Comparative Investigation of Diagnosis Media for Induction Motor: A Case of Rotor Cage Faults," *IEEE Trans. on Industry Electronics*, Vol. 47, No 5, pp. 1092–1099, Oct. 2000.
- [12] R. Maier, "Protection of Squirrel Cage Induction Motor Utilizing Instantaneous Power and Phase Information," *IEEE Trans. on Industry Applications*, Vol. 28, No 2, pp. 376–380, March/April 1992.
- [13] M. Benbouzid, "A Review of Induction Motors Signature Analysis as a Medium for Faults Detection," *IEEE Trans. on Industrial Electronics*, Vol. 47, No 5, pp. 984–993, Oct. 2000.
- [14] M. Drif and N. Benouzza and J.A. Dente, "Rotor Cage Detection in 3-Phase Induction Motors Using Instantaneous Power Spectrum," *Electrimacs'99*, pp. 287–292, 1999.
- [15] M.S. Bartlett, "Smoothing Periodograms from Time Series with Continuous Spectra," *Nature*, London, vol. 161, pp. 686-687, May 1948.
- [16] S.L. Marple, "Digital Spectral Analysis with Applications," *Prentice-Hall*, New Jersey, 1987.
- [17] G. Didier and H. Razik and O. Caspary and E. Ternisien, "Rotor Cage Fault Detection in Induction Motor using global modulation index on the Instantaneous Power Spectrum," *SDEMPED'03*, Atlanta, August 2003.
- [18] M. Haji, and H.A. Toliyat, "Pattern Recognition - A Technique for Induction Machines Rotor Broken Bar Detections," *IEEE Trans. on Energy Conversion*, Vol. 16, No. 4, Dec. 2001, pp. 312-317.
- [19] W. Deleroi, "Broken Bar in Squirrel-Cage Rotor of an Induction Motor. Part I: Description by Superimposed Fault-Currents," *Archiv Fur Elektrotechnik*, Vol. 67, pp. 91–99, 1984.
- [20] G. Didier, "Modélisation et diagnostic de la machine asynchrone en présence de défaillances," *PhD Thesis, University of Nancy*, 2004.
- [21] K. Kim, A. G. Parlos and R. M. Bharadway, "Sensorless Fault Diagnosis of Induction Motors," *IEEE Trans. on Industrial Electronics*, Vol. 50, No 5, pp. 1038–1051, Oct. 2003.

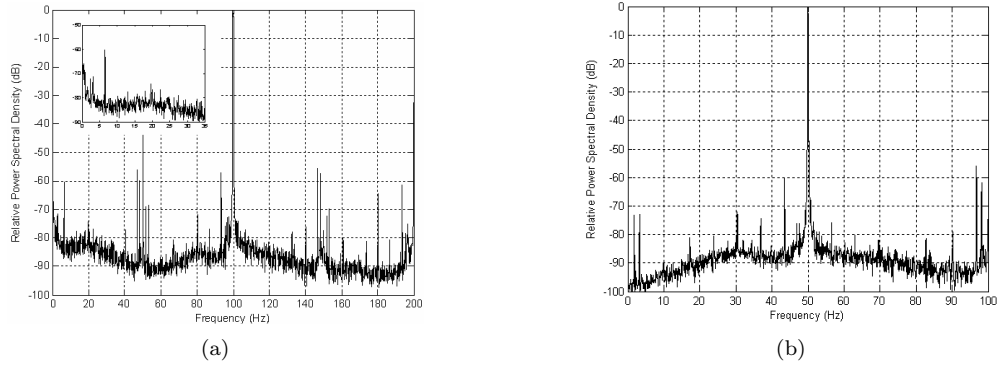


Figure 5: Bartlett periodogram of instantaneous power (a), and line current (b) for a healthy rotor (100% load).

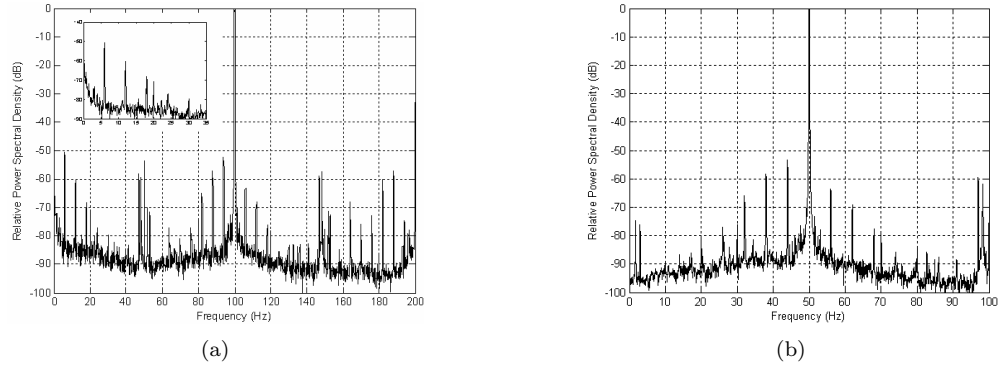


Figure 6: Bartlett periodogram of instantaneous power (a), and line current (b) for a partially broken bar (100% load).

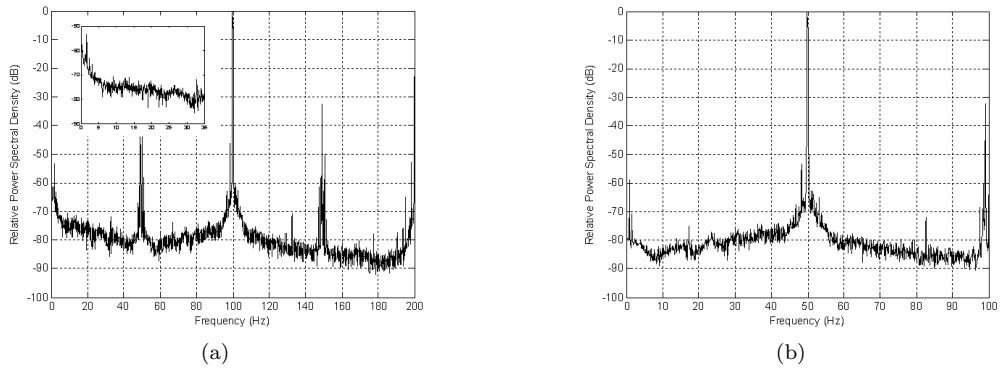


Figure 7: Bartlett periodogram of instantaneous power (a), and line current (b) for a healthy rotor (25% load).

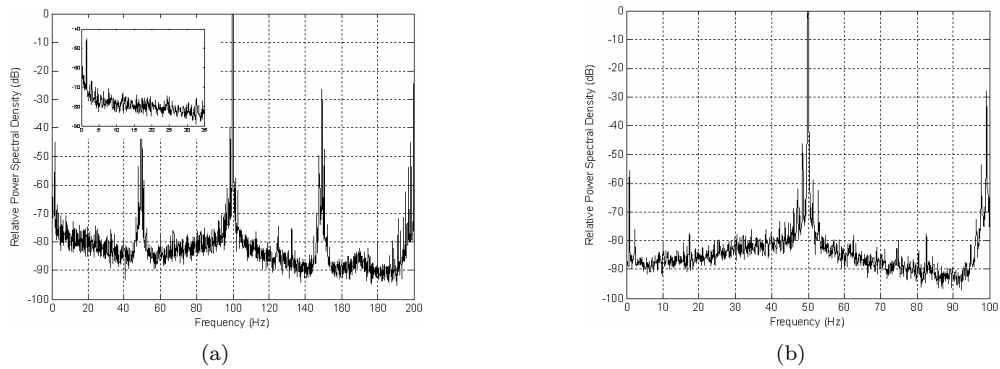


Figure 8: Bartlett periodogram of instantaneous power (a), and line current (b) for a partially broken bar (25% load).